Airway Tree Reconstruction Based on Tube Detection

Christian Bauer[1,2], Thomas Pock[1], Horst Bischof[1], and Reinhard Beichel[2,3,4]

[1] Inst. for Computer Graphics and Vision, Graz University of Technology, Austria
[2] Dept. of Electrical and Computer Engineering
[3] Dept. of Internal Medicine
[4] The Iowa Institute for Biomedical Imaging
The University of Iowa, Iowa City, IA 52242, USA
{cbauer, pock, bischof}@icg.tu-graz.ac.at
reinhard-beichel@uiowa.edu

Abstract. We present an automated approach for airway tree reconstruction from CT images. Our approach performs an initial identification of tubular structures, followed by a reconstruction of the airway tree. During the reconstruction step, tubular objects that are part of the airway tree are identified and linked together based on prior knowledge about the structure of human airway trees. A major advantage of our approach is that it handles local disturbances robustly, as demonstrated by our experiments.

1 Introduction

Segmentation of airway trees in lung CT data is a prerequisite for several clinical applications including diagnosis and monitoring of lung disease or surgical planning. To facilitate such applications, it is highly desirable to have an automated airway segmentation method which is robust. The main challenges in the context of airway tree segmentation are: noise, inhomogeneous appearance of the airway wall due to partial volume effects, motion artifacts, or lung disease (e.g., emphysema).

In the literature, several airway tree segmentation methods have been presented. An overview is given in the survey of Sluimer et al. [1], and newer approaches are discussed in [2]. Frequently, region growing or front propagation methods [3–5] are utilized that make some assumptions about the density (gray-values) of airways in CT data. More sophisticated variants of front propagation methods try to avoid segmentation errors by constantly analyzing local segmentation results and by adapting parameters accordingly. Different approaches have been proposed [3, 6, 4] that utilize local information like radius or branching angle. To enhance robustness, compared to methods that solely rely on density/gray-value information for airway segmentation, some approaches focus on airway candidate detection using mathematical morphology [7], template matching techniques [8], or voxel classification based on different image descriptors [9, 10].

Many of the available approaches have problems in dealing with local disturbances (e.g., motion artifacts) or pathology (e.g., obstructed airway) which frequently results in incomplete airway segmentations. Graham et al. [2] addressed this problem by building an airway tree from candidate airway branch segments by computing connection costs between branches and using graph theoretic approaches to extract the airway tree [2]. However, their method does not consider possible connections in the context of the complete airway tree structure which can lead to false connections.

In this work, we present an automated approach for the reconstruction of airway trees that is robust against local disturbances which can result from disease or imaging artifacts, for example.

2   Method

Our method consists of two main processing steps. First, all tubular structures are identified in the dataset. Second, the airway tree is reconstructed from these tubular objects by utilizing knowledge about the tree structure. During this step, tubular objects that are not related to airways are discarded. In addition, tubular objects that are part of the airway tree are linked together. Consequently, potential gaps between airway branches, that may occur due to disturbances (e.g., imaging artifacts), are closed. Fig. 1 illustrates the individual processing steps by showing intermediate results.

2.1   Detection and Description of Tubular Objects

Airways form tubular tree structures that can be detected by utilizing a tube detection filter (TDF), because in CT data, the airway branches appear as elongated structures with varying diameter that are darker than the surrounding tissue. To detect and describe these structures, a TDF combined with a centerline extraction method based on a ridge traversal is utilized.

The utilized multi-scale TDF extends the works presented in [11, 12]. Specifically, our method achieves an increased robustness and minimizes artifacts by utilizing additional constraints. Therefore a radius dependent tube-likeliness measure $R(\mathbf{x}, r)$ is computed for every point $\mathbf{x}$ in the image domain for a set of different radii. To obtain $R(\mathbf{x}, r)$ for a given radius r, an offset medialness function and an adaptive threshold are used that utilize two different scales simultaneously: $\sigma_{\mathcal{H}} = r$ and $\sigma_{\mathbf{B}} = r^{\eta}$ with $0.0 \leq \eta \leq 1.0$. While the scale $\sigma_{\mathcal{H}}$ is large and and is used to cover the whole structure, $\sigma_{\mathbf{B}}$ is smaller and is utilized for obtaining boundary information. First, the Hessian matrix $\mathcal{H}(\mathbf{x}) = \sigma_{\mathcal{H}}^2 \left[(\partial^2 I^{(\sigma_{\mathcal{H}})})/(\partial_{x_i} \partial_{x_j}) \right]$ with its associated eigenvalues $|e_1| \geq |e_2| \geq |e_3|$ and eigenvectors $\mathbf{v}_1$, $\mathbf{v}_2$, and $\mathbf{v}_3$ is computed, where $I^{(\sigma)} = G_\sigma \star I(x)$ corresponds to the original image at scale σ. Based on this information, "dark" structures (low density) are identified ($e_1 > 0$ and $e_2 > 0$). For these points, an offset medialness function is computed based on boundariness contributions b_i which are sampled along a circle in the tubes cross sectional plane defined by $\mathbf{v}_1$ and
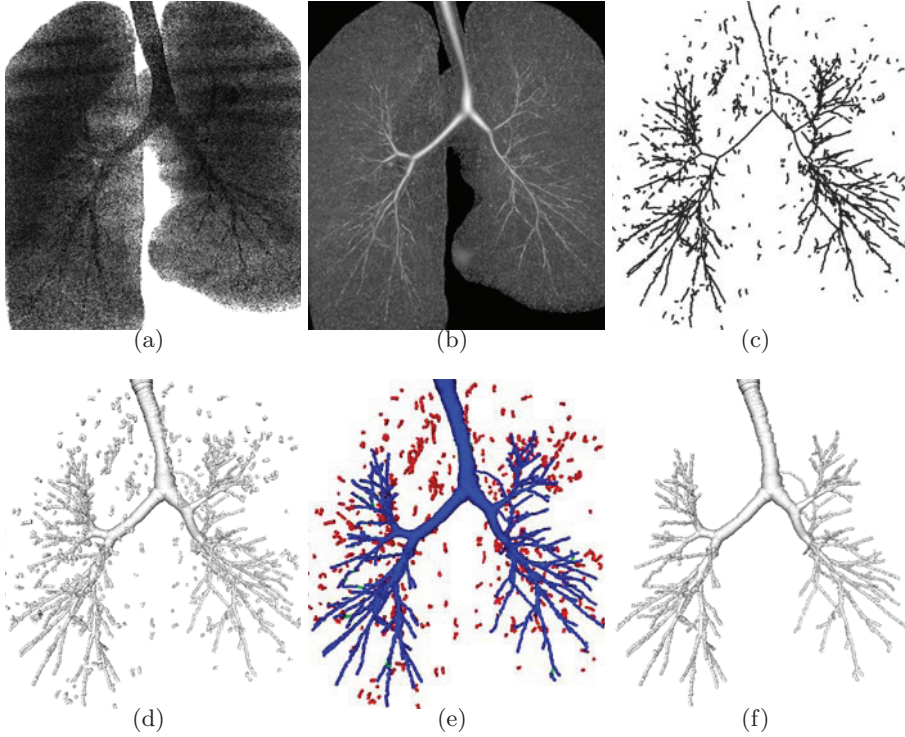
Fig. 1. Illustration of the processing steps of our airway tree reconstruction approach. (a) Volume rendering of the utilized dataset. (b) Tube detection filter response. (c) Centerlines of initially extracted tubular objects. (d) Initially extracted tubular objects with associated radii/tangent directions. (e) Tree reconstruction step showing the identified tubular objects belonging the airway tree (blue), the discarded tubular objects (red), and the closed gaps (green). (f) Reconstructed airway tree.

$\mathbf{v}_2$. The boundariness contributions are calculated at $N = \lfloor 2\pi r + 1 \rfloor$ points with varying angle $\alpha_i = (2\pi i)/N$ (N is limited to the range 16-100). The individual boundariness values $\mathbf{B}(\mathbf{x}) = \sigma_{\mathbf{B}} \nabla I^{(\sigma_{\mathbf{B}})}(\mathbf{x})$ represent a measure for the contribution of the gradient in the radial direction $\mathbf{v}_{\alpha_i} = \cos(\alpha_i)\mathbf{v}_1 + \sin(\alpha_i)\mathbf{v}_2$ of the tube: $b_i = |B(\mathbf{x} + r\mathbf{v}_{\alpha_i})\mathbf{v}_{\alpha_i}|$. Based on the average $\bar{b}(\mathbf{x}, r) = \frac{1}{N}\sum_{i=0}^{N-1} b_i$ and the variance $s^2(\mathbf{x}, r) = \frac{1}{N}\sum_{i=0}^{N-1}(b_i - \bar{b})^2$ of these boundariness samples, the offset medialness function is computed: $R_0(\mathbf{x}, r) = \bar{b}(\mathbf{x}, r)(1 - s^2(\mathbf{x}, r)/\bar{b}(\mathbf{x}, r)^2)$. The second term that includes the variance allows suppressing responses for not circular symmetric structures. To avoid wrong responses that could occur near edges, an adaptive thresholding scheme based on the gradient magnitude is used to suppress such responses, and the final medialness response for a given radius is computed: $R(\mathbf{x}, r) = \max\{R_0(\mathbf{x}, r) - \sigma_{\mathcal{H}}|\nabla I^{(\sigma_{\mathcal{H}})}(\mathbf{x})|, 0\}$. The mutli-scale response $R_{multi}(\mathbf{x}) = \max_{r_{min} \leq r \leq r_{max}}\{R(\mathbf{x}, r)\}$ is obtained as the maximum

response over all radii, which also yields the associated radius r and tangent direction $t = \mathbf{v}_3$ for each point.

An example of the TDF response is shown in Fig. 1(b). The response increases towards the tube center. Consequently, the tubular objects form ridges. As can be seen in Fig. 1(b), the filter enhances dark tubular structures (airways) without producing artifacts or responses to other image structures like the lung surface, for example. However, the response decreases in proximity of junctions, and is lower for thin low contrast airways. Consequently, separating the tubular structures from noise based on a simple global thresholding would not be robust. To address this issue, a ridge traversal procedure with a hysteresis thresholding scheme is utilized to extract centerlines. The centerlines are then analyzed and noise induced responses are discarded. The procedure requires a starting point $\mathbf{x}_0$ for every ridge and an estimate of its tangent direction which is provided by the TDF. All local maxima in the TDF response with a value $R_{multi}(\mathbf{x}) > t_{high}$ are considered as starting points and used for initialization of the traversal. Starting from a given point $\mathbf{x}_0$, the ridge is traversed in both directions $\mathbf{t}_0$ and $-\mathbf{t}_0$. Given a point on the ridge $\mathbf{x}_i$, the next point $\mathbf{x}_{i+1}$ on the ridge in the traversal direction $\mathbf{t}_i$ is chosen as the local neighbor $\mathbf{x}_i^n$ with the highest value of $R_{multi}(\mathbf{x}^n)$ that satisfies $\overrightarrow{\mathbf{x}_i \mathbf{x}_i^n} \cdot \mathbf{t}_i > 0$. The traversal direction $\mathbf{t}(\mathbf{x}_{i+1}) = \text{sign}(\overrightarrow{\mathbf{x}_i \mathbf{x}_{i+1}} \cdot \mathbf{t}(\mathbf{x}_{i+1}))\mathbf{t}(\mathbf{x}_{i+1})$ is updated to maintain the correct direction, and the procedure is repeated as long as $R_{multi}(\mathbf{x}_{i+1})$ stays above a given threshold t_{low} or an already traversed point is found. Thus, object centerlines $\{l^j\}_{j=1}^m$ are extracted for all tubular objects, consisting of an ordered set of points $\{l^j\}_{j=1}^m$ with associated radius r_i^j and tangent directions $\mathbf{t}_i^j$. To discard short spurious responses (noise), all centerlines with an accumulated TDF response below t_{conf} are discarded. For the remaining centerlines the radius and tangent directions are re-estimated by averaging over the ± 5 local neighbors along the centerline. The centerlines are split into subparts at local angles larger than $90°$ to guarantee that at furcations at least one of the centerlines has an endpoint. This is a necessary prerequisite for the next processing step. The angle is determined based on the ± 5 local neighbors along the centerline.

Figs. 1(c) and (d) depict the resulting descriptions of the identified tubular objects. Fig. 1(c) shows only the centerline information, while in Fig. 1(d) also the associated radius and tangent direction are displayed using a cylinder with appropriate orientation and radius. As can be seen, major parts of the airway tree can be extracted with this approach. However, two problems remain that have to be addressed. First, the centerlines of the tubular objects may break up at junctions or in disturbed regions (e.g., motion artifacts). Second, some false positive responses caused by other low density (dark) tube-like structures that are not airways are also present.

2.2   Tree Reconstruction

For reconstruction of the airway tree, tubular objects that are part of the actual airway tree need to be identified, and all other unrelated tubular objects must

be discarded. For this purpose, the structure and the relation between the identified tubular objects is analyzed. In addition, prior knowledge is utilized for the reconstruction. Starting from the trachea, the airway tree furcates recursively. At furcations, the radius of the child branches decreases. In addition, no abrupt changes of the tangent direction occur. Our method incorporates this knowledge. Beginning with the trachea, tubular objects that follow this pattern are merged.

During the tree reconstruction process, a graph-based representation of the whole tree is derived, describing the tree structure. In this graph, nodes represent branchpoints and edges correspond to tubular objects connecting these branch points. For all tubular objects l^j, the average radius r^j is determined and the proximal/distal direction of the tube element $d^j \in \{+1, -1\}$; $d^j = +1$ if the direction is from the first centerline point to the last or $d^j = -1$ otherwise. In addition, we define the angles $\alpha^l = \angle\big(\overrightarrow{\mathbf{x}_k^l \mathbf{x}_i^j}, d^l t_k^l\big)$ and $\alpha^j = \angle\big(\overrightarrow{\mathbf{x}_k^l \mathbf{x}_i^j}, d^j t_i^j\big)$ and the distance $d = \max\big(0, |\overrightarrow{\mathbf{x}_k^l \mathbf{x}_i^j}| - r_k^l\big)$ between points $\mathbf{x}_i^j$ and $\mathbf{x}_k^l$ of the tubular objects which are required for the tree reconstruction process. (Fig. 2).
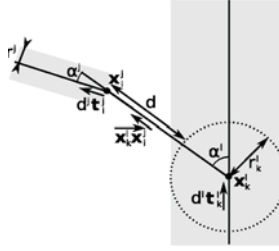

Fig. 2. Branch angles and the distance between tubular structures as used by the tree reconstruction.

Starting from the trachea, the airway tree is reconstructed by iteratively merging unconnected tubular objects. Therefore, connection confidences are calculated between endpoints of unconnected tubular objects and the current airway tree: $c(\mathbf{x}_i^j, \mathbf{x}_k^l) = exp(-\alpha^j/2\rho^2)(1 + d/r^j)$. This confidence decreases with increasing distance and increasing angle. In addition, to be considered a valid connection, the following constraints have to be fulfilled:

1. the branching angle must not be too large ($\alpha^j \leq \gamma_a$ and $\alpha^l \leq \gamma_a$),
2. the radius must not increase ($r^j \leq \gamma_r r_m$; where r_m is the smallest radius on the whole path from the trachea),
3. the connection distance must not be too large ($d \leq \gamma_d$), and
4. a minimum connection confidence is required ($c \geq \gamma_c$).

After determination of the connection with the highest confidence that fulfills all above described constraints, the associated tube element is added to the airway tree and the structural representation is updated. In addition, the identified connection is also added to the airway tree by using a linearly interpolated

path. By applying the method recursively, gaps between unconnected airway branches are closed and a connected skeleton of the whole airway tree is obtained, which includes additional radius and tangent direction for each centerline point (Figs. 1(e) and (f)).

2.3 Preprocessing Steps for Automated Airway Tree Reconstruction

The above outlined principle is general applicable. To fully automate the approach for airway detection, the input CT dataset is preprocessed to discard non lung tissue and to restrict the search area for tubular objects. Therefore a rough lung mask is generated by using thresholding ($< -700HU$), connected component analysis, and morphological closing with a ball structuring element with a radius of 10 voxels. All voxels outside this lung mask or with a value larger than $-700HU$ in the original dataset are set to $-700HU$. The resulting dataset was used as input for our method. The trachea is identified automatically by searching for the largest tubular object located at the center of the volume.

3 Evaluation

Our approach was applied to 40 clinical datasets (with undisclosed gold standard) which were provided by the organizers of the "Extraction of Airways from CT 2009 (EXACT09)" workshop (http://image.diku.dk/exact). The datasets were split in two groups of 20 training datasets, where the parameters have been adapted and 20 testing datasets. For information about how the reference segmentations were obtained and the exact definition of the used performance measures we refer to http://image.diku.dk/exact/information.php.

The following parameter were used to process the test datasets. The tube detection was performed on 15 radius steps on a logarithmic scale between radii $0.25mm$ and $10mm$ with $\eta = 0.7$ (the variance term of the boundariness samples in the offset medialness function was omitted for radii $\leq 0.5mm$); $t_{high} = 35$, $t_{low} = 25$ and $t_{conf} = 150$ for the centerline extraction; $\rho = 0.5$, $\gamma_a = 90°$, $\gamma_r = 1.3$, $\gamma_d = 40mm$ and $\gamma_c = 0.1$ for the tree reconstruction.

For evaluation, binary volume datasets were required that contain a single 6-connected airway structure. Our airway tree reconstruction method produces a 26-connected airway tree skeleton with corresponding radius information. Thus, to obtain a binary volume dataset, we performed an inverse distance transformation to obtain a rough segmentation and dilated the so obtained reconstruction to assure 6-connectivity. The generated segmentations were sent to the organizers, who in return provided evaluation results. Table 1 summarizes the evaluation results for the 20 testing datasets. On average, 57.9% of airway branches were detected with an average detected tree length of 55.2%. The mean leakage count was 6.5, and the mean false positive rate was 2.44% (median: 1.41%).

Table 1. Evaluation results on the twenty test cases.

	Branch count	Branch detected (%)	Tree length (cm)	Tree length detected (%)	Leakage count	Leakage volume (mm^3)	False positive rate (%)
CASE21	100	50.3	54.6	49.4	1	102.5	1.09
CASE22	296	76.5	258.7	78.3	23	1311.2	3.91
CASE23	232	81.7	201.0	77.2	14	700.5	2.81
CASE24	148	79.6	121.0	74.4	5	288.7	1.18
CASE25	157	67.1	134.0	53.2	9	1693.0	6.08
CASE26	39	48.8	29.4	44.7	4	254.1	5.13
CASE27	38	37.6	27.6	34.1	1	56.8	1.08
CASE28	70	56.9	50.9	46.5	2	8.6	0.09
CASE29	118	64.1	83.6	60.5	3	222.6	1.56
CASE30	91	46.7	70.2	46.0	1	47.6	0.32
CASE31	100	46.7	73.8	42.0	1	64.7	0.38
CASE32	125	53.6	118.6	54.4	2	34.8	0.14
CASE33	117	69.6	99.1	67.4	15	931.2	7.56
CASE34	296	64.6	233.5	65.3	6	167.3	0.49
CASE35	187	54.4	133.2	43.1	2	123.3	0.57
CASE36	239	65.7	283.0	68.7	8	661.1	2.12
CASE37	96	51.9	82.8	46.6	5	360.2	2.25
CASE38	40	40.8	30.8	46.3	2	79.6	1.25
CASE39	210	40.4	198.1	48.4	8	745.7	2.61
CASE40	237	60.9	219.6	56.7	17	3678.0	8.07
Mean	146.8	57.9	125.2	55.2	6.5	576.6	2.44
Std. dev.	81.8	13.0	80.3	12.8	6.3	864.9	2.46
Min	38	37.6	27.6	34.1	1	8.6	0.09
1st quartile	91	46.7	54.6	46.0	2	64.7	0.49
Median	122	55.6	108.8	51.3	5	238.3	1.41
3rd quartile	237	69.6	219.6	68.7	14	931.2	5.13
Max	296	81.7	283.0	78.3	23	3678.0	8.07

4   Discussion

In this paragraph, we discuss properties of our approach based on two examples. In Fig. 3, a case with emphysema is shown. Several structures that are similar to airways are present in the image data. They are hard to distinguish solely based on gray-value appearance. Without utilizing prior knowledge about the structure of airway trees, a correct segmentation is hard to achieve, and simple algorithms will likely show leakage. As shown in Fig. 3(b), our approach initially also identifies some of these structures as tubular objects. However, the constraints incorporated into the tree reconstruction step successfully prevent that such structures are added to the airway tree (Fig. 3(d)). In the example shown in Fig. 4, a tumor infiltrates the airway wall and blocks one of the lower airway branches completely, such that the airway tree appears to be unconnected in the image data. Contrary to region growing or front propagation approaches, our approach identifies the unconnected airways and allows us to link them together. This ability enables our method to handle local disturbances robustly.
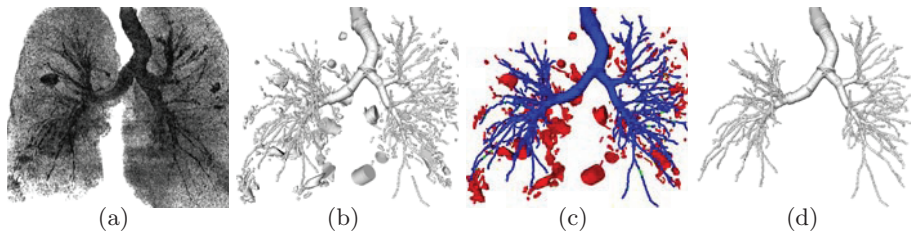

(a)   (b)   (c)   (d)

Fig. 3. Emphysema lung CT data. (a) Volume rendering of the dataset. (b) Identified tubular objects. Note that some of the "pathological" structures have been detected as tubular objects. (c) Tree reconstruction step showing the identified tubular objects belonging to the airway tree (blue), the discarded tubular objects (red), and the closed gaps (green). (d) Reconstructed airway tree.

Compared to other methods, we achieve a good trade-off between "branch count"/"tree length" and leakage. Fig. 5 depicts the three cases with the largest "leakage volume". Two points can be observed: i) the majority of the "leaks" detected by the workshop organizers are due to surface representation inaccuracies (Figs. 5(c) and (d)) and ii) blobs are included in some airway segmentations (Figs. 5(a) and (b)). Point i) can be explained as follows. Our approach produces a description of the airway tree on a structural level (centerline points, radius, tangent direction), but not a voxel or sub-voxel accurate segmentation of the inner and/or outer airway wall(s). In addition, since results were required to be 6-connected, we decided to dilate our results, which clearly negatively impacts leakage performance metrics. As shown in Fig. 5(d), voxels are classified as leakage, if the segmentation is thicker than the reference segmentation even if its structure is correct. Point ii) was caused by a bug in the software that
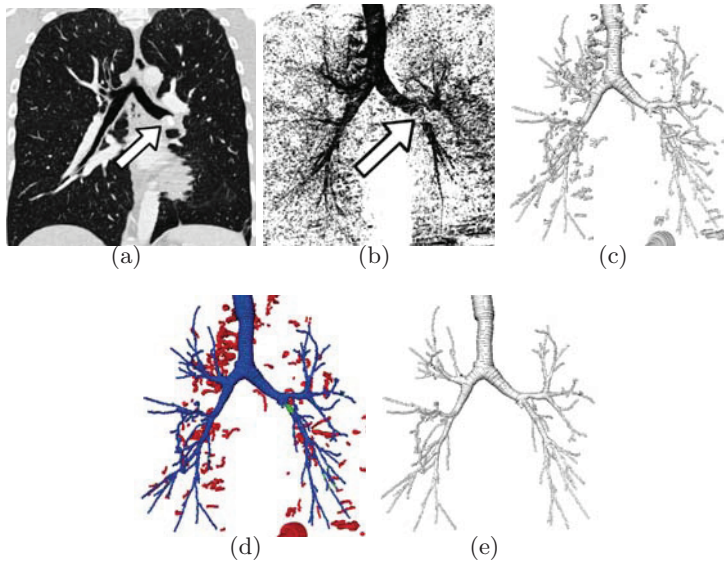
Fig. 4. Dataset with a large tumor that infiltrates and blocks one airway branch completely (indicated by the arrow). Note the gap between the airway branches at the tumor region. (a) Coronal slice of the dataset. (b) Volume rendering of the dataset. (c) Identified tubular objects showing also a gap between airway branches. (d) Tree reconstruction step showing the identified tubular objects belonging the airway tree (blue), the discarded tubular objects (red), and the closed gaps (green). (e) Reconstructed airway tree.

transformed our structural airway description into the binary volume dataset which was discovered after the evaluation. In the future we plan to improve our method by adding a surface segmentation step. The generated structural information will be utilized as a shape prior to constrain a consecutive segmentation step. The presented methods for tube detection, centerline extraction, and tree reconstruction are generic and can be utilized in other application domains.

Compared to simple airway segmentation approaches (e.g. region growing) our approach is more complex. However, TDFs as used with our approach are highly parallelizeable and well suited for a GPU (graphics processing unit) based implementation. Using a CUDA[1] based implementation of the TDF running on an NVIDIA Tesla C1060 card, the TDF response is computed on average in approximately 30 seconds per scale for the whole dataset. Using axis aligned subvolumes that just contain the lung area, computation time can be reduced to about 10 seconds per scale. The Processing time for preprocessing, ridge traversal, and tree reconstruction combined are about 30 seconds. Overall, computation time using such a subvolume containing only the lung is about 3 minutes.
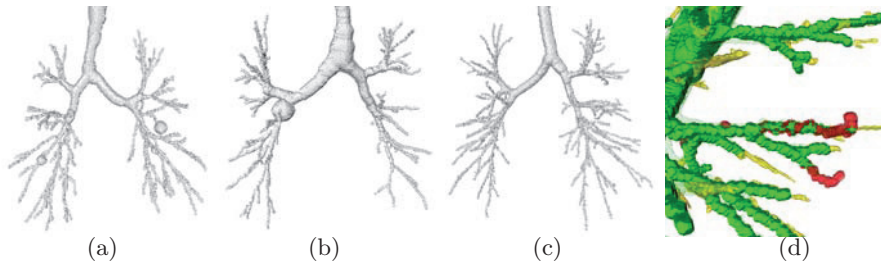
---

[1] `http://www.nvidia.com/object/cuda_home.html`

Fig. 5. Examples of reconstructed airways with a high "leakage volume". (a) CASE40: "leakage count"=17; "leakage volume"=3678.0 mm^3. (b) CASE25: "leakage count"=9; "leakage volume"=1693.0 mm^3. (c) CASE22: "leakage count"=23; "leakage volume"=1311.2 mm^3. (d) CASE22 comparison to gold standard: voxels classified as leakage (red), correct voxels (green), missed airways (yellow).

5 Conclusion

In this work we presented an automated approach for the reconstruction of airway trees from CT datasets. The approach utilizes local appearance information in combination with prior knowledge about the structure of airway trees. It first identifies tubular objects which are then grouped together to form an airway tree. As demonstrated on examples, our approach allows to robustly deal with cases where parts of the airway tree are locally disturbed.

6 Acknowledgments

References

1. Sluimer, I., Schilham, A., Prokop, M., van Ginneken, B.: Computer analysis of computed tomography scans of the lung: A survey. IEEE Trans. Med. Imag. **25**(4) (Apr. 2006) 385–405
2. Graham, M.W., Gibbs, J.D., Higgins, W.E.: Robust system for human airway-tree segmentation. In: Proc. of SPIE Med. Imag. (Mar. 2008)
3. Schlathalter, T., Lorenz, C., Carlsen, I., Reinisch, S., Deschamps, T.: Simultaneous segmentation and tree reconstruction of the airways for virtual bronchoscopy. In: Proc. of SPIE Med. Imag. (2002) 103–113
4. van Ginneken, B., Baggerman, W., van Rikxoort, E.M.: Robust segmentation and anatomical labeling of the airway tree from thoracic CT scans. In: Proc. of MICCAI, New York, USA (Sep. 2008) 219–226
5. Fabianska, A.: Two-pass region growing algorithm for segmenting airway trees from MDCT chest scans. Comput. Med. Imaging Graphics **23**(11) (Nov. 2009) 1353–1364

6. Tschirren, J., McLennan, G., Hoffman, E., Sonka, M.: Intrahotacic airway trees: Segmentation and airway morhoplogy analysis from low-dose CT scans. IEEE Trans. Med. Imag. **25**(4) (Apr. 2006) 385–405

7. Fetita, C.I., Preteux, F., Beigelman-Aubry, C., Grenier, P.: Pulmonary airways: 3-D reconstruction from multiscale CT and clinical investigation. IEEE Trans. Med. Imag. **23**(11) (Nov. 2004) 1353–1364

8. Swift, R.D., Kiraly, A.P., Sherbondy, A.J., Austin, A.L., Hoffman, E.A., McLennan, G., Higgins, W.E.: Automatic axis generation for virtual bronchoscopic assessment of major airway obstructions. Comput. Med. Imaging Graphics **26**(2) (2002) 103 – 118

9. Sato, Y., Nakajima, S., Atsumi, H., Koller, T., Gerig, G., Yoshida, S., Kikinis, R.: 3D multi-scale line filter for segmentation and visualization of curvilinear structures in medical images. In: CVRMed-MRCAS. (1997) 213–222

10. Lo, P., de Brujine, M.: Voxel classification based airway tree segmentation. In: Proc. of SPIE Med. Imag. (Mar. 2008)

11. Krissian, K., Malandain, G., Ayache, N., Vaillant, R., Trousset, Y.: Model-based detection of tubular structures in 3D images. CVIU **2**(80) (2000) 130–171

12. Xu, M., Pycock, D.: A scale-space medialness transform based on boundary concordance voting. J. Math. Imaging Vision **11**(13) (Dec 1999) 277–299